Stress stability and thermo-mechanical properties of reactively sputtered alumina films

M. P. HUGHEY, R. F. COOK
Department of Chemical Engineering and Materials Science, University of Minnesota, Minneapolis, Minnesota 55455

J. THURN
Advanced Mechanical Technology, Mechanical Research and Development, Seagate Technology, Bloomington, Minnesota 55435

Published online: 25 October 2005

The stability of residual stress inherent on deposition in reactively sputtered alumina films is studied during thermal cycling and annealing, simulating temperature excursions experienced by the films during device fabrication and subsequent operation. Increasing the magnitude of substrate bias applied during deposition acts to reduce the amount of argon incorporated in the films; more incorporated argon corresponds to smaller values of modulus and hardness and a larger coefficient of thermal expansion (CTE). Large, irreversible changes in film stress develop on heating, acting to decrease the compressive residual stress of films deposited on silicon substrates to a smaller, equilibrium value, whereas films deposited on Al_2O_3-TiC substrates behave differently. Thermal cycling and annealing have little effect on the modulus and CTE, but the hardness increases significantly and the threshold load for indentation crack initiation decreases precipitously during heat treatment. Possible mechanisms of irreversible stress development and mechanical property modifications are discussed.
© *2005 Springer Science + Business Media, Inc.*

1. Introduction
Alumina (AlO_x) films can be deposited by many techniques, such as evaporation [1, 2], r.f. non-reactive sputtering [3, 4], d.c. reactive sputtering [4, 5], and r.f. reactive sputtering [4, 6]. For many applications, amorphous alumina is desired, and such material finds applications in optical [6, 7], electrical [3, 8], and similar devices, and finds significant usage in the magnetic recording industry by serving as the basecoat and thick protective overcoat in the recording head [9] and possibly as the transducer dielectric [10]. In these cases, the alumina serves in merely an insulating or passivating role, but the film stress and thermo-mechanical properties are important. Protective films must be tough, stiff, and have small coefficients of thermal expansion (CTE); a small compressive stress is desired, and stress stability is required. Primarily, an engineer would like to know and control thermo-mechanical properties and film stress to help identify and control pole-tip recession and thermal pole tip protrusion—common irreversible and reversible deformation that can limit magnetic recording head performance [10–12].

Amorphous alumina films for use in thin film magnetic recording heads are primarily deposited by non-reactive sputtering from polycrystalline Al_2O_3 targets. A common feature of such films is the incorporation of the sputtering gas—typically argon—which tends to scale with the physical properties of the film, including the residual compressive stress [13]. It is known that in alumina and similarly prepared materials the amount of incorporated sputtering gas typically increases with increasing magnitude of substrate bias (voltage difference between substrate and plasma) applied during deposition, which in turn corresponds to greater compressive stress [13, 14]. Previous work has shown that the residual stress in alumina deposited by non-reactive sputtering becomes more compressive on annealing or thermal cycling when deposited on glass [15] or polycrystalline Al_2O_3-TiC [16], but becomes slightly less compressive when deposited on Si [16]. Here, the thermo-mechanical properties and behavior of alumina films deposited by reactive sputtering (sputtering in the presence of a reactive gas) from metallic Al targets are studied to test their suitability in magnetic recording head applications.

2. Experimental procedure
Aluminum oxide, or alumina, films were deposited on Si (100) and polycrystalline Al_2O_3-TiC (64% Al_2O_3, 35% TiC, 1% additives, wt%) substrates by dual r.f./d.c. reactive magnetron sputtering from an aluminum target. The sputtering atmosphere was composed of argon and oxygen in a 9:1 ratio at a total pressure of 4.5 mTorr; the average deposition rate was 311 Å/min.

0022-2461 © *2005 Springer Science + Business Media, Inc.*
DOI: 10.1007/s10853-005-2070-0

The sole processing parameter varied was r.f. substrate bias, and films were deposited on silicon using four different voltages: –50, –100, –150, and –200 V. Films were deposited on Al_2O_3-TiC at –50 and –75 V. The intended film thickness on silicon was approximately 8.6 μm, except for films deposited at –100 V, which were 4.4, 8.6, or 18 μm thick; films deposited on Al_2O_3-TiC were approximately 20 μm thick. Film thickness was measured with a spectroscopic reflectometer (NanoSpec, Nanometrics) using a 25-point pattern and confirmed on a few cross-sectioned samples using scanning electron microscopy (SEM) with a field-emission gun (JSM-6500F, JEOL).

Optical measurements of wafer curvature were performed with commercial instruments (FSM900TC, Frontier Semiconductor and Flexus 2320, Tencor), and film stress was calculated using the Stoney equation [17] for biaxial film stress, σ_f:

$$\sigma_f - \sigma_0 = (\kappa - \kappa_0)\frac{E_s t_s^2}{6(1 - \upsilon_s)t_f}, \qquad (1)$$

where σ_0 is room-temperature film stress immediately after film deposition (the "deposition" stress), κ is wafer curvature, κ_0 is room-temperature wafer curvature immediately after film deposition, E_s is the substrate Young's modulus (168.9 GPa for Si [18] and 390 GPa for Al_2O_3-TiC [19]), υ_s is the substrate Poisson's ratio (0.064 for Si [18] and 0.22 for Al_2O_3-TiC [19]), t_s is substrate thickness, and t_f is film thickness. The value of σ_0 was unknown until the curvature of the bare substrate was measured after all thermal cycling and annealing (κ_{final}), allowing the determination of final film stress from which the deposition stress was calculated; the films were removed by etching with concentrated KOH. During curvature measurements, the substrates were rotated by up to 135 °, and differences of up to 30 MPa for film stress were sometimes observed depending on wafer orientation. Films were thermally cycled in vacuum at 3°C/min to peak temperatures up to 400°C. The typical temperature program was as follows: heating to 100°C and back to room temperature twice; heating to 200°C and back twice; heating to 300°C, annealing at constant temperature for 3 h, and cooling to room temperature; heating to 400°C, annealing for three hours, and cooling to room temperature. Stress measurements were recorded at 10°C intervals below 100°C and at 25°C intervals above 100°C; data were recorded every six minutes during constant temperature annealing.

Several films were deposited at each value of substrate bias, allowing for mechanical testing on some wafers and wafer curvature measurements on others. Multiple test samples approximately 1 cm square were cut from silicon wafers intended for mechanical testing. Some of these samples were placed in the wafer curvature apparatus at the same time as the "twin" wafer in order to receive identical thermal treatment; samples were removed at various times during the thermal cycling. Additionally, some films were used for both types of experiments by cleaving a wide strip from the middle of the wafer for curvature measurements, and by using the remainder of the wafer for mechanical testing. The following describe experiments conducted on the small samples. A depth-sensing indentation (DSI) apparatus (Nano Indenter XP, MTS Systems) was used to measure the hardness, H_f, and the plane-strain Young's modulus, E_f^*, of the films, where $E_f^* = E_f/(1 - \upsilon_f^2)$ and E and ν are defined as before with the subscript "f" indicating a film property. These experiments were performed with a well-calibrated Berkovich diamond tip and continuous stiffness measurements [20]. The Young's modulus was calculated by assuming a film Poisson's ratio of 0.2. The CTE, α_f, of the films was calculated by using the slope of the stress-temperature data in the thin film approximation:

$$\alpha_f = \alpha_s - \frac{(1 - \upsilon_f)}{E_f}\frac{d\sigma_f}{dT} \qquad (2)$$

where α_s is the substrate CTE (calculated from Si data [21] as 2.87×10^{-6} K^{-1} and measured by thermomechanical analysis as 6.0×10^{-6} K^{-1} for Al_2O_3-TiC, both averaged over 25–100°C) and T is the temperature. Hardness of the films was also measured from conventional Vickers indentations performed with gravity-loaded indenters (Micromet 2100, Buehler and Model 3212, Zwick) at loads ranging from 0.1 to 60 N and observed with a visible light microscope (Epiphot 200, Nikon). The residual half-diagonal, a, of the Vickers impression was measured, giving $H_f = P/2a^2$ where P is the load. To ensure substrate-independent responses, values of modulus and hardness were obtained from data corresponding to a maximum contact depth (depth of the material-indenter contact region) of less than 10% of the film thickness for the modulus [22, 23] and less than 40% of the film thickness for the hardness [23]. The Vickers hardness impressions as well as gravity-loaded indentations made with a cube-corner indenter were used to evaluate fracture properties of the film.

The elemental composition of the films was measured by Rutherford backscattering spectrometry (RBS) using 2 MeV $^4He^+$ ions (accelerator: 5SDH, National Electrostatics Corporation; analytical endstation: RBS 400, Charles Evans & Associates). SEM was used to study the film structure: in cross-section, a 1.0 kV accelerating voltage was utilized; for plan-view imaging, the samples were coated with ~50 Å of Pt and 5.0 kV was used. The crystallinity of the films was investigated by X-ray diffraction (XRD) using Cu$K\alpha$ radiation (Bruker-AXS D5005, Siemens).

3. Results

3.1. Characterization

The deposition conditions described above led to the formation of thick, amorphous films, as confirmed by XRD. The as-deposited films were shown by RBS to contain substantial amounts of argon, as is commonly observed in biased reactive sputtering of alumina [5], but can be avoided with proper choices of deposition parameters (including target type and choice of magnetron or diode configuration) [4]. The amount of incorporated argon increased with increasing substrate

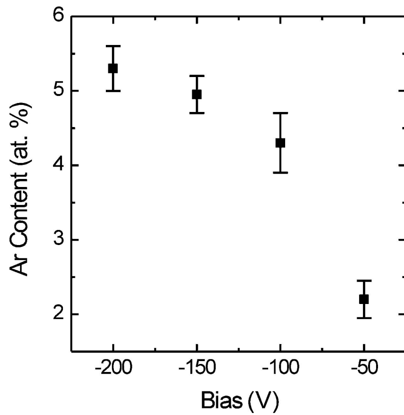

Figure 1 Incorporated argon content in alumina films vs. substrate bias applied during deposition.

bias magnitude, from 2.2 at.% at –50 V to 5.3 at.% at –200 V, as shown in Fig. 1. The trend of argon versus bias is nonlinear, with a large difference between the amount of argon in the –50 V film and the amount in the –100 V film. The O/Al atomic ratios were approximately 1.43 for each film; slightly oxygen deficient films are commonly observed [3, 16], but the O/Al ratio can range from 1.3 to 1.9 [4, 5]. Although the incorporation of the heavier argon atom would seem to lead to an increase in density, the mass density estimated from RBS measurements was nearly invariant at 2.3 g/cm^3, which is comparable to measured densities of some amorphous alumina films [24] and small relative to others [3, 8, 25]. (The mass density was invariant as a result of increased argon incorporation being associated with smaller atomic densities.) Ignoring the small difference in density or O/Al ratio among the films, the only significant difference in the structure or composition was the amount of incorporated argon.

The Young's modulus was observed to decrease with increasing bias magnitude. This trend is described more effectively by plotting the modulus versus the material parameter—the argon content. As shown in Fig. 2, the modulus decreases nearly linearly with increasing argon content; no effect of film thickness or substrate type was observed. The values are in the range 140–160 GPa, which is comparable to values for other sputtered alumina films [25–27]. Also shown in Fig. 2 is the film CTE averaged over 25–100°C; these values were calculated from stress-temperature data, which were typically linear over small temperature ranges. The CTE also followed an approximately linear trend with argon content—independent of film thickness—increasing from about 4.2 to 5.5$\times10^{-6}$ K^{-1} as the argon content increases from 2.2 to 5.3 at.%. Few CTE values for alumina films have been reported in the literature, but the values shown here are comparable to, if slightly smaller than, previous freestanding film measurements of 5.2–6.1$\times10^{-6}$ K^{-1} (obtained via analysis of published strain-temperature data [15]) and film-on-substrate measurements of 5.2–5.8$\times10^{-6}$ K^{-1} (recalculated from Refs. [16] and [27] with an Al_2O_3-TiC CTE of 6.0$\times10^{-6}$ K^{-1} and corrected film moduli). The increase of CTE with argon incorporation could be expected: argon thermal expansivity ($\alpha_p = V^{-1}(\partial V/\partial T)_p \sim 3\alpha$, with V the molar volume and p the pressure) is very large in either the compressed gas or solid phase. (At room temperature, α_p for fluid argon is calculated to be approximately 5$\times10^{-4}$ K^{-1} at 1 GPa from data in Ref. [28] and α_p for crystalline argon is calculated to be approximately 3$\times10^{-4}$ K^{-1} at 2 GPa from data in Ref. [29].) However, it is not clear that the variation in CTE is due entirely to argon content, as a simple rule-of-mixtures between alumina and argon predicts much larger values for the film CTE for all observed values of argon content.

Measured hardness values were in the range 7.7–8.4 GPa for conventional Vickers indentation and 9.5–9.9 GPa for DSI with a Berkovich indenter. These are in the range observed for alumina films [26, 27], but are substantially smaller than the largest claimed values [5]. The hardness did not show a definitive trend with argon content, although it appeared to decrease slightly with increasing argon, as shown in Fig. 3 (open bars) for Vickers indentation results; again, no effect of film thickness or substrate type was observed. The consistently larger values obtained by ultra small-scale DSI (or "nanoindentation") with a Berkovich indenter are in accordance with measurements of other systems, particularly alumina films deposited by non-reactive sputtering [27]. The difference is likely attributed to the calibration of the DSI area function to the modulus, not hardness, of soft, compliant materials such that

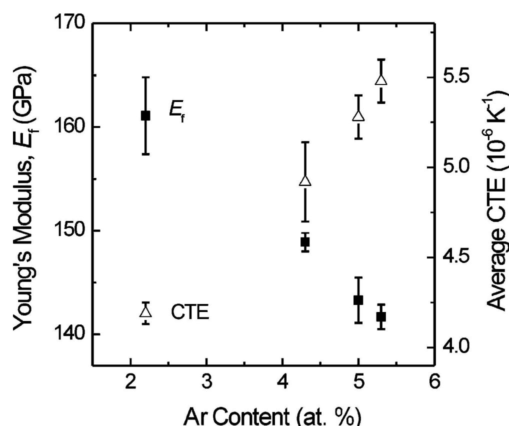

Figure 2 Film Young's modulus (closed squares) and CTE average over 25–100°C (open triangles) vs. incorporated argon content.

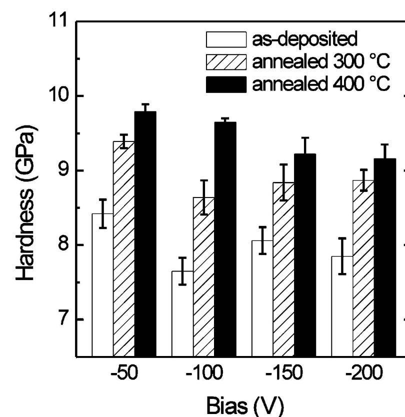

Figure 3 Film Vickers hardness for each applied substrate bias, showing the increase in hardness for the as-deposited films (open) as they are annealed at 300°C (hatched) and 400°C (closed).

the contact area is systematically underestimated (and thus resistance to plastic deformation overestimated) for stiff, hard materials such as these alumina films [30].

The threshold load for crack initiation (the load at which some designated percentage of indentations cause radial cracking) provided insight into the fracture behavior of the films. Following convention, this indentation cracking threshold was defined as the load at which cracking occurred for at least 60% of the potential cracking sites (corners of the indentation impression) using a total of at least five Vickers indentations, i.e., for at least 12 potential cracking sites if five indentations are performed [31]. The indentation cracking threshold load was a function of substrate type, film thickness, and substrate bias. Threshold loads for films deposited on Al_2O_3-TiC were 1 N and 5 N for substrate biases of –50 V and –75 V, respectively. The apparent hardness was constant for all loads at or below the threshold, indicating that the substrate—which is much harder than the films—did not influence the indentation response. On silicon, larger threshold loads were observed. The hardness of silicon and the films are approximately equal, preventing ready determination of any substrate influence. However, the threshold was so large for most films that the corresponding contact depth—equal to $a/3.5$—was nearly equivalent to the film thickness; thus, the silicon substrate was cracking under the indentation load. The influence of the silicon substrate is illustrated in Fig. 4. A sub-threshold indentation is depicted in Fig. 4a: while the indentation load is applied (left), a region of plastically deformed material—which may extend into the substrate—is created, but a critical defect does not nucleate. After the load is removed, no cracks propagate. However, as shown in Fig. 4b, when the load is increased such that the contact depth is nearly equivalent to the film thickness, crack nuclei form in the brittle silicon near the interface with the film. After the load is removed, these cracks propagate in both the substrate and the film. A large dependence of the threshold load on film thickness in films deposited at –100 V confirmed this influence of the silicon substrate: for film thicknesses of 4.4, 8.6, and 18 μm, the threshold loads were 4, 12, and 39 N, respectively. (In each case, the contact depth was approximately equal to the film thickness.) Thus, the film was merely an impediment to substrate fracture, and the true threshold of a film deposited at –100 V could be at least 39 N—substantially larger than the value for a film deposited at –50 V.

Although the measured threshold loads for films deposited on silicon substrates were not independent of the substrate, the effect of deposition bias was still evident in these data, as the threshold load for 8.6 μm thick films decreased from 14 N at –100 V to 3 N at –50 V. Very little effect of bias was observed for a bias magnitude greater than –100 V (i.e., Fig. 4b corresponds to threshold indentations in –100 V, –150 V, and –200 V films of any thickness on silicon). The 3 N threshold load for films deposited at –50 V corresponded to a contact depth equal to about half of the film thickness, such that cracks nucleated in the film—near the surface where the stresses that drive radial cracks are largest [32, 33]—as illustrated in Fig. 4c. That this was greater than the threshold load of the same film deposited on Al_2O_3-TiC is likely because the film deposited on silicon was much thinner, such that plastic deformation in the substrate altered the driving force for radial crack initiation; for a thick film on Al_2O_3-TiC, the deformation is contained within the film. The difference in film stress between different films (see Section 3.2) did not appear to affect the threshold load, as there was very little difference in threshold at large bias, and the application of a fracture model for indentation crack initiation [31] indicated that a difference in film stress was unlikely to explain much of the difference in behavior between films deposited at –50 V and –100 V. In an attempt to decrease the threshold load, a cube-corner indenter was also used to investigate the fracture properties; however, the threshold was not decreased sufficiently to avoid influence of the substrate.

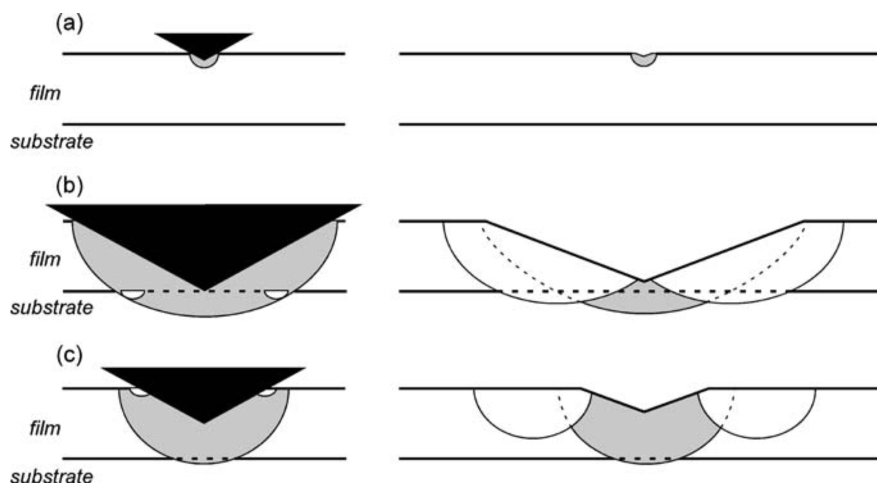

Figure 4 Schematic cross-sections of Vickers indentations in films deposited on silicon during the contact event (left) and after load removal (right). (a) For a sub-threshold load indentation, a plastically deformed region is created, but cracking does not initiate. (b) For a threshold load in films deposited at –100 V, –150 V, and –200 V, the contact depth is approximately equal to the film thickness and cracks nucleate in the substrate near the film interface. (c) For a threshold load in films deposited at –50 V, the contact depth is significantly less than the film thickness and cracking initiates in the film near the surface. The plastically deformed region extends well into the substrate in (b) and may extend into the substrate in (a) and (c).

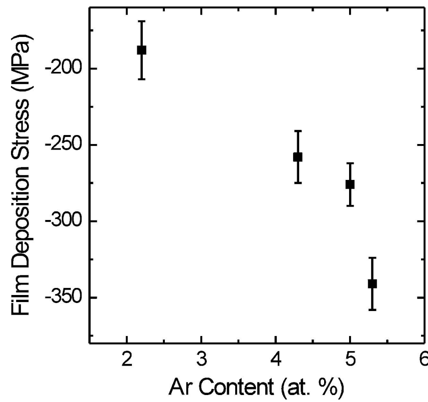

Figure 5 Deposition film stress vs. incorporated argon content.

3.2. Film stress

Films deposited by reactive sputtering ("reactive" films) had as-deposited stress values ranging from approximately –190 MPa at –50 V to –340 MPa at –200 V—much larger values of compression than observed previously in similar films deposited by non-reactive sputtering ("non-reactive" films) [16]. The deposition stress magnitude increased with increasing argon content—or increased with increasing bias magnitude—as shown in Fig. 5. Over a smaller range of argon content, no correlation between argon content (or deposition bias) and deposition stress was observed in non-reactive films [16]. Regardless of stress magnitude, generic changes in stress were observed on thermal cycling. Specifically, the film stress changed in two ways on thermal cycling: (1) reversibly and nearly linearly with temperature due to thermal strain mismatch caused by a difference between the film and substrate CTE; and (2) irreversibly and nonlinearly with temperature at temperatures greater than about 100–125°C.

Shown in Fig. 6 are stress-temperature data for a film deposited at –50 V on Si. The room-temperature deposition stress is –188 MPa. On heating to 100°C, the stress becomes more compressive due to the film CTE being greater than that of the substrate; this change is reversible and nearly linear with temperature. On heating to a temperature greater than about 125°C, the residual stress changes irreversibly and nonlinearly with temperature, becoming less compressive. After one cycle to 200°C, the residual stress is 23 MPa less compressive than the deposition stress—that is, cycling to 200°C brought about 23 MPa of stress hysteresis. Subsequent cycles to 200°C exhibited only reversible thermal stress. Thermal cycles to higher temperatures lead to similar effects: cycling to 300°C with a three hour anneal at the peak temperature brought about an additional 48 MPa of stress hysteresis, and identical cycling to 400°C led to an additional 45 MPa. The residual stress after all thermal cycling is –72 MPa—still compressive, but less compressive than the as-deposited state because of +116 MPa of stress hysteresis. The kinetics of stress change can be examined by plotting film stress versus time during the constant-temperature anneals, as is shown in the figure inset. Due to the compressive thermal stress, the value of stress at the beginning of each anneal is nearly identical. In addition, the total stress change during each anneal is nearly equivalent. For both anneals, the data appear to behave according to a decaying exponential function of time, indicative of first-order kinetics:

$$\Delta\sigma_{\mathrm{f}} = \Delta\sigma_{\mathrm{f,T}} \exp(-t/\tau), \qquad (3)$$

where $\Delta\sigma_{\mathrm{f}}$ is irreversible film stress change, $\Delta\sigma_{\mathrm{f,T}}$ is a fitting constant that corresponds to the predicted stress change at infinite time, t is time, and τ is the time constant and the inverse of a rate constant. The primary difference between the annealing data at the two different temperatures is that the kinetic rate is greater at 400°C as judged by a smaller time constant for the decaying exponential fit to the data and can be observed from the much greater initial rate of stress change for the higher temperature anneal. (Time constants varied greatly for the different films, with no obvious trend with bias, but averaged 59 min at 300°C and 38 min at 400°C.) Finally, note that stress continued to increase, albeit slowly, at the end of each three hour anneal.

These data can be contrasted with stress-temperature data for a film deposited at –200 V on Si, shown in Fig. 7. This film was deposited in much greater compression (–340 MPa), and the reversible stress-temperature slope is much steeper, indicating a greater

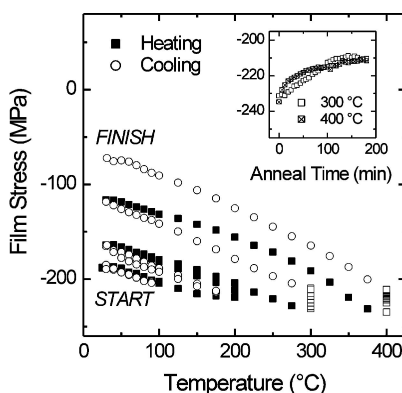

Figure 6 Film stress vs. temperature for an alumina film deposited at –50 V on Si and thermally cycled (closed squares and open circles) and annealed (open squares). The inset displays film stress vs. time during three-hour anneals at 300°C and 400°C.

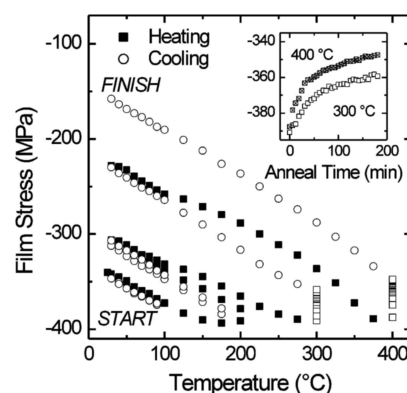

Figure 7 Film stress vs. temperature for an alumina film deposited at –200 V on Si and thermally cycled (closed squares and open circles) and annealed (open squares). The inset displays film stress vs. time during three-hour anneals at 300°C and 400°C.

CTE (given the comparable modulus values) than that of the film deposited at –50 V. Again at around 125°C, film stress begins to change irreversibly and nonlinearly with temperature. After one cycle to 200°C, 28 MPa of stress hysteresis has developed, and repeated cycles show only reversible stress changes. Cycling to and annealing at 300°C and 400°C brought about 84 MPa and 71 MPa of stress hysteresis, respectively. The total stress hysteresis was 183 MPa—much greater than was observed for the film deposited at –50 V—leaving the film with a residual film stress of –158 MPa. Once again, the figure inset displays the kinetic behavior of stress change during the constant temperature anneals. Similarly to the previous data, data for the film deposited at –200 V are very similar at the two temperatures, with a greater rate of change for the higher temperature data, and stress continued to change at the end of the anneals; however, the stress change at 400°C is 9 MPa greater than at 300°C for this film.

The behavior of films deposited on Al_2O_3-TiC is very different, as shown in Fig. 8 for a film deposited at –50 V. The reversible stress-temperature slope is now positive because the substrate CTE is larger than the film CTE. More importantly, the film stress begins to change irreversibly at around 100°C and actually becomes more compressive during heating and a subsequent two-hour anneal at 160°C, resulting in a final film stress of about –213 MPa. The total magnitude of irreversible stress change during this cycle and anneal was approximately equal in magnitude, but opposite in sign, to that of a –50 V film on silicon cycled to 200°C. A film deposited at –75 V and cycled in the same manner exhibited essentially no irreversible stress change.

A summary of irreversible stress change behavior for films deposited on silicon (and cycled in the same manner) is shown in Table I, averaged for each deposition substrate bias. The irreversible stress change is given for each cycle, listed by the peak temperature, and the total for all thermal cycling. Note that one film deposited at –100 V was thermally cycled with the reverse anneal sequence: 400°C first (which was accompanied by a very large stress hysteresis), followed by 300°C (which caused no irreversible stress change, possibly indicative of metastable equilibrium behavior). The stress hysteresis during each cycle (and thus the total irreversible stress change) was much less for films deposited at –50 V; there was no discernible trend between substrate bias and irreversible stress change for the other films. Furthermore, reversing the anneal sequence had no effect on the total irreversible stress change, confirming that the rate of stress change is rapid enough that the ∼30 min required to heat from 300 to 400°C were sufficient to make up for the lack of the three hour 300°C anneal.

TABLE I Film stress hysteresis summary

Bias (V)	200°C $\Delta\sigma_f$ (MPa)	300°C $\Delta\sigma_f$ (MPa)	400°C $\Delta\sigma_f$ (MPa)	Total $\Delta\sigma_f$ (MPa)
−50	25	45	45	115
		70	70	180
−100	40	0†	145†	185
−150	35	70	70	175
−200	40	75	70	185

†Cycled to 400°C first, then to 300°C.

As stress was observed to increase at the end of every three hour anneal, a very long-time anneal was performed to explore any equilibrium behavior. Stress-time data are shown in Fig. 9 for a film deposited at –100 V (on Si); the film was thermally cycled in the same manner as the other films, but the 400°C anneal was extended to 21 h. The majority (∼75%) of the change in stress occurred during the first 3 h of the anneal. These data also can be fit reasonably well by a decaying exponential function of time. Most importantly, however, is that the residual stress remained constant (at a value of about –230 MPa) after approximately 16 h. Although no other films were annealed for such a long time, the annealing data indicated that they were all tending towards a constant compressive value.

3.3. Changes in film properties on heating

The large irreversible changes in film stress are clearly brought about by permanent changes in the film structure. All characterization efforts described in Section 3.1 were duplicated after the completion of thermal cycling, as well as after the 300°C annealing

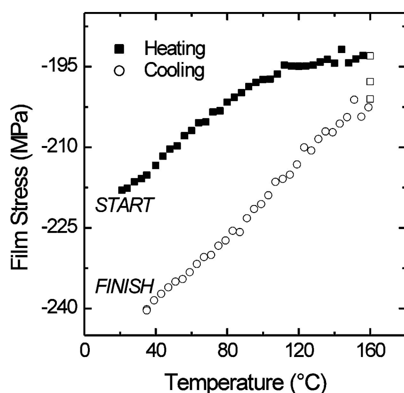

Figure 8 Film stress vs. temperature for an alumina film deposited at –50 V on Al_2O_3-TiC and heated (closed squares), annealed for three minutes at 160°C (open squares), and cooled (open circles)

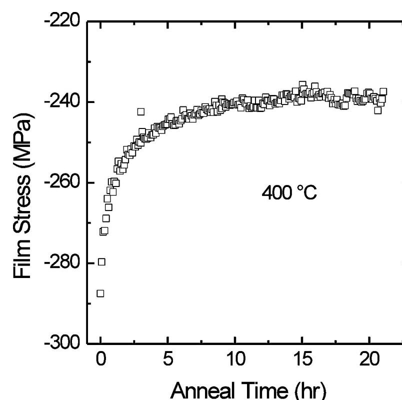

Figure 9 Film stress vs. time for an alumina film deposited at –100 V (on Si) and annealed at 400°C for 21 h. The data demonstrate zero change in stress after approximately 16 h.

cycle in some cases. Cross-sectional SEM showed that any change in film thickness was limited to less than the resolution of the film-substrate interface and the film edge (∼0.5% of the film thickness). XRD performed on annealed samples indicated the films remained amorphous at these temperatures, as expected from much previous investigation of alumina films [15, 34, 35]. RBS experiments showed no change in film stoichiometry; importantly, no argon escaped from the film at these temperatures, confirming previous work on similar films [15, 16]. The elastic properties of the films changed very little, with insignificant increases in Young's modulus and CTE observed. However, large changes in the hardness were observed. A comparison of Vickers hardness in the as-deposited state (open bars), after annealing at 300°C (hatched), and after annealing at 400°C (solid) is shown in Fig. 3. After each annealing step, the hardness increased significantly; total increases from the as-deposited state to after all thermal cycling and annealing were 1.5–2 GPa. Analogous increases were observed with DSI, with the values all larger by nearly 2 GPa.

The fracture behavior of the films also changed greatly on annealing, as seen in Fig. 10: the Vickers indentation cracking threshold load for films deposited on silicon was reduced by a factor of 2–3, while the threshold load either stayed constant or increased slightly for films deposited on Al_2O_3-TiC. (Films deposited on Al_2O_3-TiC were annealed at 300 and 400°C for mechanical testing, although film stress was only recorded for a maximum temperature of 160°C.) The films deposited on Al_2O_3-TiC are 20 μm thick and only films approximately 8.6 μm thick deposited on silicon are shown, although the same phenomenon was observed for all films deposited on silicon. As before, the threshold for films deposited on silicon was nearly invariant with bias except at –50 V. For films deposited at greater bias magnitudes, the contact depth was reduced to less than the film thickness, meaning fracture initiated in a manner akin to Fig. 4c. However, the substrate still influenced the measurement, as film thickness again played a role for films deposited at –100 V: the threshold loads (and contact depths as a percentage of film thickness) were 2 N (65%), 5 N (50%), and 12 N (40%) for 4.4, 8.6, and 18 μm thick films, respectively. The decreasing relative contact depth at the threshold with increasing thickness indicates that 12 N is very near the true post-annealing threshold. The direction of changes in the threshold matched the direction of irreversible stress change: compressive film stress acts to suppress cracking, thus a reduced compressive stress could result in a reduced threshold. However, the application of a fracture model for indentation crack initiation [31] suggests that the reduction in film stress (for films deposited on silicon) was unlikely to explain the reduction in the threshold. The increase in hardness would also be expected to decrease the threshold load [31], although if this were the cause of the threshold decrease for films deposited on silicon, it does not explain the results for films deposited on Al_2O_3-TiC. Other important factors that could be expected to cause a decrease in the threshold load are a decrease in toughness and an increase in the crack nucleus (which forms inside the contact impression) size [31].

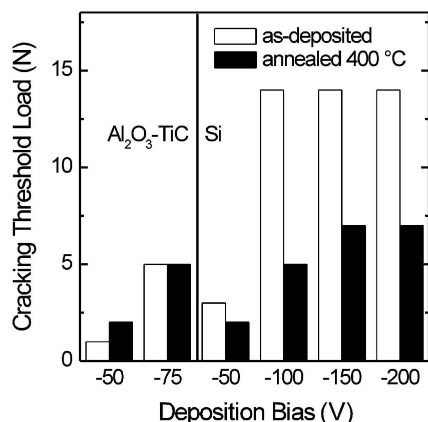

Figure 10 The threshold load for crack initiation for films deposited on both substrates, before and after annealing. The threshold is greatly reduced in films deposited on silicon (all 8.6 μm thick, although the effect was observed in all films), but not greatly affected in films deposited on Al_2O_3-TiC (20 μm thick).

SEM was also used to study indentation fracture in as-deposited and annealed (at 400°C) films deposited on silicon. Images are shown in Fig. 11 for 14 N indentations made in a 8.6 μm thick film deposited at –100 V; this is slightly greater than the threshold load of the as-deposited film (left) and significantly greater than the threshold load of the annealed film (right). A dramatic difference is observed in the deformation zones of the contact impressions. For the as-deposited sample, the deformed region is smooth and homogeneous, and the surface traces of the radial cracks are observed to lie within the impression by a length of approximately 0.05 a. The annealed film appears very different: the deformed region is very heterogeneous near the impression edges, with visible shear faults intersecting the surface and running parallel to the edges. The radial cracks—which form at the intersection of shear faults [36, 37]—lie further within the impression, at a total length of about 0.13 a. These observations are consistent with observations of indentation deformation in various glasses: permanent deformation in "normal" glasses—such as soda-lime glass—is volume conserving through the inhomogeneous failure of material via shearing, whereas permanent deformation in "anomalous" glasses—which contain a substantial amount of free volume, such as fused silica—has a large non-volume conserving component through densification mechanisms [38]. Thus, at least some of the deformation in the as-deposited films (deposited on silicon) appears to be accommodated by non-volume conservation processes (i.e. densification) whereas deformation in the annealed films is mostly volume conserving; this change could be driven by a reduction in the amount of free volume in the films. Other things being equal, less free volume would result in greater hardness, as was observed on annealing. This also suggests that the harder films deposited at –50 V have less free volume and would be expected to show more shear faulting than other films, perhaps even before annealing; however this was not observed in a limited number of indentations studied with SEM.

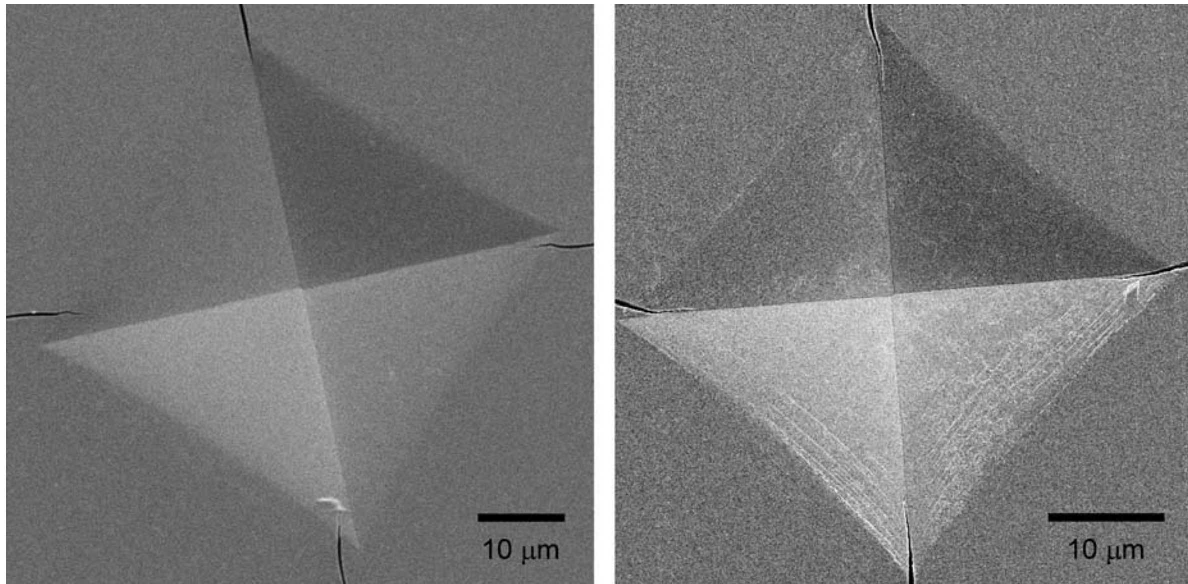

Figure 11 SEM micrographs of 14 N Vickers indentations in an 8.6 μm thick alumina film deposited on Si at –100 V. Compared with the as-deposited sample (left), the sample annealed at 400°C (right) is observed to exhibit extensive shear faulting, which is accompanied by decreased indentation cracking threshold and increased hardness.

4. Discussion

4.1. Mechanics and thermodynamics of transformation

The mechanism responsible for the large irreversible changes in residual stress is unclear, especially given the very different behavior of presumably identical films deposited on different substrates, as well as the different behavior of very similar films (reactive vs. non-reactive) on identical substrates. The large change towards less compression for reactive films on silicon substrates here is in opposition to the change towards greater compressive stress observed for reactive alumina on Al_2O_3-TiC substrates or non-reactive alumina on glass [15] and Al_2O_3-TiC substrates [16], and much larger than previously observed compressive stress mitigation for non-reactive alumina on silicon substrates [16]. (The films on silicon studied in Ref. [16] exhibited ~32 MPa of stress hysteresis towards less compression when cycled and annealed in the same manner up to 400°C as the films studied here [39].) Despite this uncertainty, general descriptions of the nature of structural transformations that occur in these films can be made.

The development of increased compressive stress implies a film is increasingly constrained from a larger unconstrained stress-free state. That is, the constraint imposes a negative strain on the film relative to the dimensions in the unconstrained state. This is what occurs during the deposition of alumina: the films are contracted by the deposition process (increasingly so as substrate bias increases) relative to the equilibrium volume the collection of atoms at this temperature and composition would occupy with the same structure. This also occurs during the heating at low temperature of alumina deposited on silicon (or the cooling of alumina deposited on Al_2O_3-TiC): the larger (smaller) CTE of the film relative to the substrate leads to an effective increased constraint on heating (cooling). In this reversible thermal expansion effect, both the constraint dimensions and the stress-free dimensions of the film are changing. This increased constraint is illustrated in the top half of Fig. 12: a film is deposited

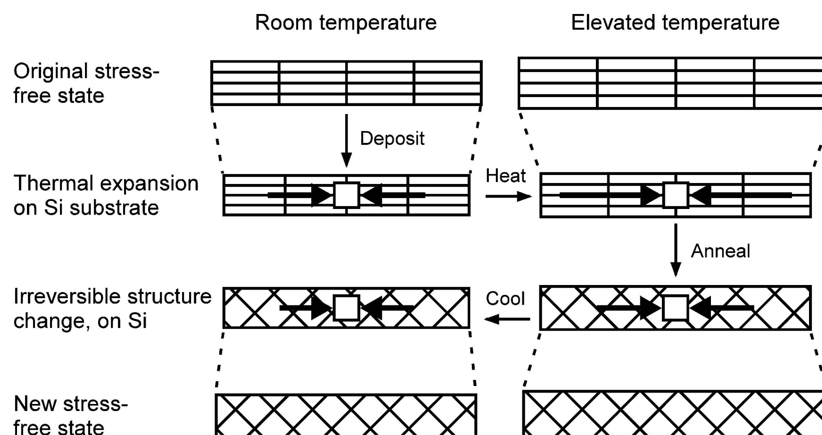

Figure 12 An illustration of the changes in constraint and stress-free dimensions that lead to increased or decreased compressive stress. The cartoon depicts a film deposited onto a silicon substrate with a compressive stress that increases on heating, but then diminishes from a structural change such that the film is constrained relative to a new equilibrium volume.

onto a silicon substrate with a compressive stress due to the film being contracted relative to the stress-free state. On heating, the film expands, but the constraint is increased because of the smaller CTE of the substrate.

Contrarily, the development of decreased compressive stress implies a film is decreasingly constrained from a larger unconstrained stress-free state. That is, the constraint imposes a still negative but decreasing strain on the film relative to the dimensions in the unconstrained state. This occurs reversibly during the cooling of alumina deposited on silicon (or the heating at low temperature of alumina deposited on Al_2O_3-TiC). This also occurs during the annealing of alumina deposited on silicon; however in this case the change in constraint arises entirely from irreversible structural changes (presumed to be localized phase transformations) in the film. As the substrate is neutral (the dimensions remain unchanged), it is more physical to describe the change in the unconstrained dimensions of the films. Because the film structure is changing irreversibly, the film is constrained relative to the now *different* equilibrium volume of a collection of atoms matching the new structure of the film. The decreasing constraint means the equilibrium stress-free volume of films deposited on silicon decreases on annealing. This is illustrated in the bottom-right quarter of Fig. 12: on annealing, the film structure changes irreversibly, and the constraint dimensions remain constant. However, the new structure corresponds to a new, smaller equilibrium volume. On cooling, the constraint is decreased further due to the thermal expansion effect.

The decrease in equilibrium film volume on annealing for films on silicon is in response to an irreversible structural transformation that would densify the film in the absence of constraint. Likewise, the equilibrium volume of films deposited on Al_2O_3-TiC increases on annealing (most obviously in non-reactive films, and here to a lesser extent) in response to an irreversible structural transformation that would decrease the film density in the absence of constraint. The opposite behavior exhibited by films deposited on silicon and Al_2O_3-TiC indicates that the irreversible structural transformations are not acting to minimize the strain-energy density, the measure of internal energy density associated with elastically strained bonds (equal to one half the product of the stress and elastic strain tensors). Likely, changes in film structure act to minimize the appropriate free energy, a component of which is the strain-energy density (as an element of the internal energy). For the constant temperature annealing of a solid object of nearly constant volume, but changing stress, the Helmholtz free energy seems most appropriate. The change in free energy, ΔA, on the phase transformation at the annealing temperature, T, is

$$\Delta A = \Delta U - T\Delta S, \tag{4}$$

where ΔS is the change in entropy on the phase transformation, and the change in internal energy, ΔU, is dominated by the change in strain energy. For alumina films deposited on silicon, the phase transformation is associated with $\Delta U < 0$, whereas $\Delta U > 0$ for the transformation of alumina films deposited on Al_2O_3-TiC. The structural transformation in films deposited on Al_2O_3-TiC must then be associated with a large $\Delta S > 0$, whereas this requirement is not necessary for films deposited on silicon, allowing for the possibility of a different phase transformation.

4.2. Comparison of film stress effects

The comparison of film stress effects for films deposited on different substrates and at different values of deposition bias may provide insight into the equilibrium behavior. The equilibrium condition shown in Fig. 9 indicates that each film could have an equilibrium stress, which could be unique to the film depending on physical parameters such as temperature, density, stoichiometry, and possibly substrate. It would be useful to compare both the magnitude of irreversible stress change (as shown in Table I, which approximates how far from equilibrium a film is at the beginning of an anneal) and the absolute value of stress during the stress change for the different reactive and non-reactive films (which indicates the approximate equilibrium stress value). This is shown in Fig. 13 for irreversible stress change occurring at 300°C. (The data for the non-reactive films are from Ref. [16].) Data for non-reactive films are shown on the left, and data for reactive films are shown on the right, and substrate deposition bias is used to differentiate the films. Arrows indicate the direction and magnitude of the total irreversible stress change at 300°C; arrows are closed for films deposited on silicon substrates, open for films deposited on Al_2O_3-TiC substrates. For non-reactive alumina films, there is no obvious difference in behavior between films deposited at –50 and –130 V. A –130 V film deposited on silicon exhibits almost no stress hysteresis, whereas the same films deposited on Al_2O_3-TiC greatly increases in compression, indicating that the equilibrium stress at 300°C is approximately –140 MPa (region indicated by shaded box).

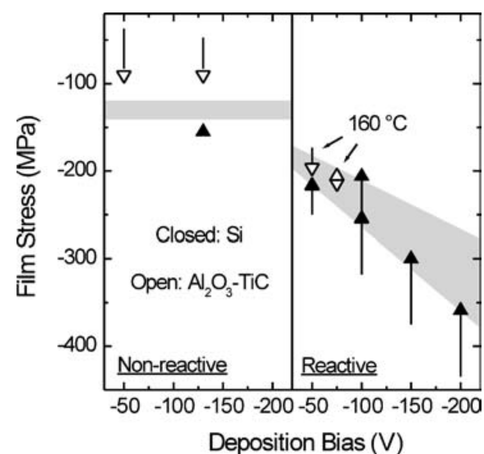

Figure 13 The change in film stress (direction and magnitude indicated by arrows) for non-reactive (Ref. [16]) and reactive alumina films on Si and Al_2O_3-TiC during annealing at 300°C (reactive alumina films on Al_2O_3-TiC were annealed at 160°C). There appears to be a unique equilibrium value of stress that each film strives to achieve; this value (estimated by the shaded regions) appears to be constant for non-reactive films but for reactive films may be a function of temperature, density, stoichiometry, or other physical parameters set by deposition.

The reactive alumina films exhibit irreversible stress change at much larger values of compression—which increase with increasing deposition bias—due to the much larger deposition stresses. It appears (perhaps by chance) that, like non-reactive films, reactive films are deposited with a film stress approximately equal to the equilibrium film stress at elevated temperature, such that irreversible stress change (at least at small bias) tends to be opposite for the two different substrates because thermal stress has caused the film stress to deviate from equilibrium in opposite directions. There appears to be a region of equilibrium stress that increases in magnitude with increasing deposition bias, as indicated by the shaded region. The films deposited at –50 V were not far from their equilibrium state, and the film deposited on Al_2O_3-TiC at –75 V was essentially in equilibrium at the annealing temperature. Films deposited at greater bias magnitudes were further from the equilibrium region, and thus experienced greater irreversible stress change. In comparing reactive films on silicon with those on Al_2O_3-TiC, one must note that the films on Al_2O_3-TiC were annealed at 160°C, not 300°C. The amount of irreversible stress change would likely be a little larger, at least for the film deposited at –50 V. However, the absolute value of stress during the change would not likely vary much, as the compressive stress change would compete with the decrease in compression that occurs on heating from 160°C to 300°C. Note that the multiple arrows and large range of stress change for films deposited at –100 V indicate the amount of variability in behavior inherent to these films. At 400°C, the situation is less clear, as the reactive films on Al_2O_3-TiC annealed at 160°C are no longer useful for comparison. However, it appears that the stress equilibrium value shifts only slightly, as was suggested by the annealing behavior shown in Figs 6 and 7.

4.3. Exsolution effects on film stress

One possible stress change mechanism, first described by Gardner *et al*. [15], involves the exsolution and diffusion of incorporated argon over small distances to voids or bubbles, allowing for the relief of structural distortions. This description, however, only provides an explanation for a stress change in one direction—either towards greater compression or less compression. Thurn and Cook extended this idea by assuming argon enters or exits voids or bubbles based on the equilibrium concentration of dissolved argon in the solid, which is affected by the film stress (pressure) [16]. In this formulation, the equilibrium dissolved concentration $X_{\mathrm{Ar}}(p, T)$ is related to the zero pressure equilibrium concentration $X_{\mathrm{Ar},0}(T)$ by

$$X_{\mathrm{Ar}} = X_{\mathrm{Ar},0} \exp\left(-\frac{p\Delta\bar{V}_{\mathrm{Ar}}}{RT}\right), \qquad (5)$$

where a positive pressure corresponds to a compressive stress, R is the universal gas constant, and $\Delta\overline{V}_{\mathrm{Ar}}$ is the change in partial molar volume on dissolution. Thus, for $\Delta\overline{V}_{\mathrm{Ar}} < 0$ (dissolved argon occupying less volume than exsolved), greater pressure (greater compression) gives rise to a greater equilibrium concentration; furthermore, exsolution of argon acts to increase the film volume in the absence of constraint, which increases compression. Implicit in this formulation is that chemical potential considerations dominate, and the strain energy is negligible compared to the total free energy. The substrate affects irreversible stress change only through the modification of the chemical potential of dissolved argon. However, it is unclear whether the pressurized bubbles of argon that are likely trapped in sputtered films [40–42] (which could also be solid [43]) could provide the necessary driving force for argon to reach equilibrium solubility in a significant portion of the film volume.

While the incorporation of argon seems likely to strongly influence the mechanical properties of these films and may be causally linked to irreversible stress change as well, the simple rearrangement of argon does not appear to be the primary driving force of stress change. This is supported by evidence of irreversible stress development in films that do not contain any incorporated noble gas, such as silicon nitride non-reactively sputtered in nitrogen [15], although it is possible for nitrogen to form bubbles as well [42]. Hence, other insights into structural transformations and their connection to the observed irreversible stress changes are needed.

4.4. Structural rearrangement effects on film stress

An alternative mechanism of irreversible stress change involves structural rearrangements, which could still allow for an equilibrium film stress and competition between the changes in strain energy and entropy associated with the phase transformation. A potential phase transformation could be related to the coordination of aluminum in the amorphous solid. While aluminum in α-alumina is octahedrally coordinated with oxygen and is in both octahedral and tetrahedral arrangements with oxygen in γ-alumina, aluminum in amorphous alumina is reported to be predominantly in tetrahedral arrangements [44, 45] or in both octahedral and tetrahedral arrangements [46]. While the films studied here remained amorphous during heating to 400°C and below, the thermal energy provided may have been sufficient for the atomic structure to rearrange and form more (or less, depending on whether the stress was increased or decreased by the rearrangement) octahedral aluminum coordination. This process would carry out (or reverse itself) until the free energy achieved was minimized, resulting in the observed equilibrium stress. The observed changes in mechanical properties may also be explained by such rearrangement. It has been proposed that hardness increases with the number of Al–O linkages [47], although this would not explain the increase in hardness of films on both substrates. A significant rearrangement in aluminum coordination could manifest itself not only in the value of hardness, but in the amount of free volume in the films. As discussed, this could alter the primary mechanism by which plastic deformation occurs, giving rise to the behavior shown in Fig. 11. Further, it is possible that significant changes

are not observed in the modulus and CTE because the increase (or decrease) in Al–O linkages is offset by the bonds being longer (shorter), mitigating their influence on the material's stiffness.

5. Summary

The stress stability and thermo-mechanical properties of reactively sputtered alumina films deposited at various values of bias magnitude on silicon and Al_2O_3-TiC substrates were studied. The only structural property that appeared to vary with bias was the amount of incorporated argon; most thermo-mechanical properties scaled with the argon content. Most of the properties were similar to those of non-reactively sputtered alumina films, and the CTE in particular was small, indicating that the films could be a suitable dielectric material for thin film magnetic recording heads. The films were deposited with a compressive residual stress that was not stable at temperatures greater than about 100°C. Films deposited on silicon became less compressive and apparently reached an equilibrium stress value during long-time anneals, whereas films deposited on Al_2O_3-TiC either became slightly more compressive or were stable at the tested temperatures. The direction of irreversible stress change matched observations of non-reactively sputtered alumina deposited on the same two substrates. Stress in alumina films appears to be driven by atomic rearrangement until an equilibrium stress has been reached, which may depend on temperature, density, stoichiometry, and other physical parameters; to reach this equilibrium, the compressive film stress may increase or decrease depending on the substrate CTE. Accompanying the large stress development for films on silicon were a substantial increase in the film hardness and a substantial decrease in the threshold load for indentation fracture, but essentially no change in the elastic modulus or CTE was observed. This appears to be consistent with the atomic rearrangement that leads to irreversible stress change, but this remains to be studied in more detail.

Acknowledgments

The authors would like to thank Seagate Technology and Unaxis for providing the films. Yongqiang Wang is also thanked for his assistance in performing RBS experiments and analyzing the results, as is Aaron Vodnick for performing some of the Vickers indentations and subsequent measurements.

References

1. L. PARFITT, M. GOLDINER, J. W. JONES and G. S. WAS, *J. Appl. Phys.* **77** (1995) 3029.
2. J. PROOST and F. SPAEPEN, *ibid.* **91** (2002) 204.
3. R. S. NOWICKI, *J. Vac. Sci. Technol.* **14** (1977) 127.
4. P. VUORISTO, T. MÄNTYLÄ, P. KETTUNEN and R. LAPPALAINEN, *Thin Solid Films* **204** (1991) 297.
5. K. KOSKI, J. HÖLSÄ and P. JULIET, *ibid.* **339** (1999) 240.
6. B. J. H. STADLER, M. OLIVERIA and L. O. BOUTHILLETTE, *J. Am. Ceram. Soc.* **78** (1995) 3336.
7. K. K. SHIH and D. B. DOVE, *J. Vac. Sci. Technol.* **A 12** (1994) 321.
8. P. VUORISTO, T. MÄNTYLÄ and P. KETTUNEN, *J. Mater. Sci.* **27** (1992) 4985.
9. M. JIANG, S. HAO and R. KOMANDURI, *Appl. Phys.* A **77** (2003) 923.
10. A. ALFOQAHA and K. YOUNG, *J. Appl. Phys.* **93** (2003) 6561.
11. W. YAN, *ibid.* **91** (2002) 7571.
12. W. W. SCOTT and B. BHUSHAN, *ibid.* **91** (2002) 8328.
13. C. A. ROSS, *J. Vac. Sci. Technol.* A **14** (1996) 2511.
14. J. H. KIM and K. W. CHUNG, *J. Appl. Phys.* **83** (1998) 5831.
15. R. A. GARDNER, P. J. PETERSON and T. N. KENNEDY, *J. Vac. Sci. Technol.* **14** (1977) 1139.
16. J. THURN and R. F. COOK, *J. Mater. Sci.* **39** (2004) 4799.
17. G. G. STONEY, *Proc. R. Soc. London* **A 82** (1909) 172.
18. W. A. BRANTLEY, *J. Appl. Phys.* **44** (1973) 534.
19. SPC Report for Material AC-72, Sumitomo Special Metals Co., Ltd. (2003).
20. W. C. OLIVER and G. M. PHARR, *J. Mater. Res.* **7** (1992) 1564.
21. R. B. ROBERTS, *J. Phys. D* **14** (1981) L163.
22. Y. SUN, T. BELL and S. ZHENG, *Thin Solid Films* **258** (1995) 198.
23. J. L. HAY, M. E. O'HERN and W. C. OLIVER, in Materials Research Society Symposium Proceedings, edited by N. R. Moody, W. W. Gerberich, S. P. Baker and N. Burnham (Materials Research Society, Warrendale, PA, 1998) Vol. 522, p. 27.
24. C. S. BHATIA, G. GUTHMILLER and A. M. SPOOL, *J. Vac. Sci. Technol.* A **7** (1989) 1298.
25. T. HANADA, H. FURUYA, S. TANABE and N. SOGA, *J. Non-Cryst. Solids* **152** (1993) 188.
26. T. C. CHOU, T. G. NIEH, S. D. MCADAMS and G. M. PHARR, *Scripta Metall. et Mater.* **25** (1991) 2203.
27. J. THURN and R. F. COOK, *J. Mater. Sci.* **39** (2004) 4809.
28. C. TEGELER, R. SPAN and W. WAGNER, *J. Phys. Chem. Ref. Data* **28** (1999) 779.
29. L. W. FINGER, R. M. HAZEN, G. ZOU, H. K. MAO and P. M. BELL, *Appl. Phys. Lett.* **39** (1981) 892.
30. J. THURN and R. F. COOK, *J. Mater. Res.* **19** (2004) 124.
31. D. J. MORRIS, S. B. MYERS and R. F. COOK, *J. Mater. Sci.* **39** (2004) 2399.
32. S. S. CHIANG, D. B. MARSHALL and A. G. EVANS, *J. Appl. Phys.* **53** (1982) 298.
33. R. F. COOK and G. M. PHARR, *J. Am. Ceram. Soc.* **73** (1990) 787.
34. J. A. THORNTON and J. CHIN, *Am. Ceram. Soc. Bull.* **56** (1977) 504.
35. P. BRÜESCH, R. KÖTZ, H. NEFF and L. PIETRONERO, *Phys. Rev.* B **29** (1984) 4691.
36. H. M. CHAN and B. R. LAWN, *J. Am. Ceram. Soc.* **71** (1988) 29.
37. R. F. COOK and L. M. BRAUN, *J. Mater. Sci.* **29** (1994) 2192.
38. A. ARORA, D. B. MARSHALL, B. R. LAWN and M. V. SWAIN, *J. Non-Cryst. Solids* **31** (1979) 415.
39. J. THURN, unpublished.
40. Z. L. LIAU and T. T. SHENG, *Appl. Phys. Lett.* **32** (1978) 716.
41. A. PRUYMBOOM, P. BERGHUIS, P. H. KES and H. W. ZANDBERGEN, *ibid.* **50** (1987) 1645.
42. L. HULTMAN, J.-E. SUNDGREN, L. C. MARKERT and J. E. GREENE, *J. Vac. Sci. Technol.* A **7** (1989) 1187.
43. G. FARACI, S. LA ROSA, A. R. PENNISI, S. MOBILIO and G. TOURILLON, *Phys. Rev.* B **43** (1991) 9962.
44. P. LAMPARTER and R. KNIEP, *Physica* B **234–236** (1997) 405.
45. G. GUTIÉRREZ and B. JOHANSSON, *Phys. Rev.* B **65** (2002) 104202.
46. A. J. BOURDILLON, S. M. EL-MASHRI and A. J. FORTY, *Philos. Mag.* A **49** (1984) 341.
47. H. L. WANG, C. H. LIN and M. H. HON, *Thin Solid Films* **310** (1997) 260.

Received 19 April
and accepted 6 May 2005